Liquid−Liquid Limited-Supply Diffusion Studies in the Polystyrene−Poly(vinyl methyl ether) Pair

J. Pablo Tomba,*,†,‡ José M. Carella,*,†,§ David García,|| and José M. Pastor||,⊥

Instituto de Investigaciones en Ciencia y Tecnología de Materiales (INTEMA) (UNMdP-CONICET), Juan B. Justo 4302, 7600 Mar del Plata, República Argentina, Departamento de Ingeniería Química, Facultad de Ingeniería, Universidad Nacional de Mar del Plata, Juan B. Justo 4302, 7600 Mar del Plata, República Argentina, Departamento de Ingeniería en Materiales, Facultad de Ingeniería, Universidad Nacional de Mar del Plata, Juan B. Justo 4302, 7600 Mar del Plata, República Argentina, Centro de Investigación y Desarrollo en Automoción (CIDAUT), Parque Tecnológico de Boecillo, Parcela 209, 47151 Valladolid, España, and Departamento de Física de la Materia Condensada, Escuela Técnica Superior de Ingenieros Industriales, Universidad de Valladolid, Paseo del Cauce s/n, 47011 Valladolid, España

Received May 10, 2003; Revised Manuscript Received April 19, 2004

ABSTRACT: Liquid−liquid diffusion at the interphase between poly(vinyl−methyl ether) (PVME) and polystyrene (PS) was experimentally studied using confocal Raman microspectroscopy. A combination of a specially designed experimental setup and a direct and precise quantification for the corrections to be applied to the Raman measurements allowed us to measure directly the PVME concentration along the diffusion path for a wide range of diffusion times. An already proposed and tested liquid−liquid diffusion model (based on liquid dynamics controlled by monomeric friction coefficients) was used to correlate and predict the detailed shape of the PVME concentration profiles and the diffusion rates as functions of diffusion time and temperature. The results obtained allowed us to discern among several approaches previously proposed in the literature to calculate monomeric friction coefficients in this system. Only the approach that considers independent monomeric friction coefficient values for PS and PVME (obtained from tracer diffusion measurements) gave good agreement between experimental results and model calculations. Calculations performed using literature data for a common monomeric friction coefficient for both PS and PVME (obtained from estimated blend viscosity data) do not agree with experimental measurements. The success of the model used for this work clearly ruled out the need for combinations of Fickean and Case II models used previously to describe PS−PVME polymer diffusion.

Introduction

Liquid−liquid diffusion in polymer pairs has received considerable attention in recent years. Besides its importance in some industrial processes, its connection with recent theories of molecular viscoelasticity has contributed to the development of successful physical models to predict quantitatively the influence of the main variables involved in the diffusion processes. Currently, it is helping to elucidate important details of the chain dynamics of individual components in miscible polymer blends.

When two miscible polymers are put in contact in the liquid state, diffusion occurs in a concentrated regime. The most interesting feature of this regime is that the motions of the diffusing species are strongly coupled with the properties of the matrix. In many cases, the physical properties of the diffusing species are different from those of the matrix, and therefore, the diffusion process produces large changes in the polymeric local environment. It usually leads to nonsymmetric interphase composition profiles.[1−3] At this point, the modeling of the process turns out more complex and the simple Fickean diffusion model with a constant diffusion coefficient becomes inadequate.[4] On the other hand, some details of the composition profiles, such as the rate of change of the composition profiles slopes along the interphase diffusion path or its overall curvature and symmetry, may reflect rich information about the polymer−polymer interaction[3,5] and are very important to understand the nature of the diffusion process.[2−4,6]

Few miscible polymer pairs have been used as models for diffusion studies in the concentrated liquid−liquid regime. Among them, the polystyrene (PS)−poly(phenylene oxide) (PPO) pair has been the most studied.[2,3,5,7,8] For this polymer pair, asymmetric interphase composition profiles have been experimentally measured and a Fickian diffusion model developed by Kramer[4] has been successfully used to predict and correlate all the experimental results.[3,7] As predicted by this model, large differences in molecular mobility along the diffusion path, originated in the large difference between the glass-transition temperatures and/or molecular weights of the pure polymers, are the cause of formation of asymmetric interphase composition profiles.[2,7]

Poly(vinyl−methyl ether) (PVME) is also miscible with PS in wide ranges of concentrations and temperatures. Some properties of their blends, miscibility curves, and separation processes have been thoroughly studied. The composition dependence of the glass-transition temperature (T_g) of PS−PVME blends has been shown not to follow the classical Fox or Gordon−Taylor equations.[9−11] Phase diagrams for wide ranges

* To whom correspondence should be addressed. E-mail: jcarella@fi.mdp.edu.ar and jptomba@fi.mdp.edu.ar.
† Instituto de Investigaciones en Ciencia y Tecnología de Materiales.
‡ Departamento de Ingeniería Química, Universidad Nacional de Mar del Plata.
§ Departamento de Ingeniería en Materiales, Universidad Nacional de Mar del Plata.
|| Centro de Investigación y Desarrollo en Automoción.
⊥ Universidad de Valladolid.

10.1021/ma0346052 CCC: $27.50
Published on Web 06/02/2004

of molecular weights and temperatures have been determined.[10−16] The temperature and composition dependence of the PS−PVME Flory−Huggins interaction parameter have been calculated.[11,14] The molecular dynamics for these blends in the liquid state has been shown to follow a general WLF-type temperature dependence.[11,17] Colby has shown that the general time−temperature superposition (TTS) principle is not obeyed for PS−PVME miscible blends if the frequency range is extended to about 10 decades, but for smaller frequency ranges, the TTS principle could be used without large errors involved.[18] PS and PVME monomeric friction factors for both species have been measured for several compositions and temperatures and shown to be very different in values.[17,19,20]

Jabbari and Peppas reported the first extensive studies on liquid−liquid PS−PVME diffusion, including the interpretation of the results in terms of mechanistic models.[21] The authors used attenuated total reflection infrared spectroscopy (ATR-FTIR) to follow the evolution of the diffusion process between a thin PS layer and a thicker PVME layer. ATR-FTIR is an indirect technique in the sense that the measured signal represents a summation of contributions originated at different depths. Furthermore, the depth range from which the IR signal was collected represents at most 15% of the total original pure PS layer thickness, which excludes the interphase.[21] The combined facts of measuring the IR signal from the least representative part of the sample and using an integral type of signal make the ATR-FTIR experimental results very hard to invert to obtain a unique interphase composition profile. To interpret the results obtained, the authors used a Fickean diffusion model with constant diffusion coefficient, which failed in predicting the time evolution of the whole diffusion process. To improve the fit of the experimental data, they resorted to using simple weighed combinations of Fickean and Case-II diffusion models.[22]

This methodology has been extensively used by the mentioned authors and by others in recently published works.[23] We believe that the use of those combinations can lead to a misleading interpretation of the physics of the diffusion process, even while—as has been shown—a Case-II contribution may improve substantially the fit of the experimental data.[21] Case-II is a model developed only for diffusion of low-molecular weight liquids into glassy polymer matrices.[24] A distinctive feature of this diffusion mechanism is that the liquid penetration is non-Fickean because it is rate-controlled by the competition between the osmotic pressure (produced by the liquid penetrant) and the mechanical relaxation of the glassy matrix. In contrast, liquid−liquid diffusion between polymer pairs that differ markedly in their T_g is a Fickean process, controlled by the diffusion of the more mobile of the two polymers.[4,6,7] However, both processes share a common characteristic: the advancing liquid species move against rapidly increasing gradients of physical properties that decrease the liquid mobility. In the Case-II regime, these properties are represented by the steep gradients of osmotic pressure and glassy matrix yield stress;[25,26] in liquid−liquid diffusion between polymers pairs that differ markedly in their T_g, they are represented by gradients of chemical potential, local T_g, and monomeric friction factors.[7] This fact makes the shapes of the advancing fronts of the composition profiles for both mechanisms to look qualitatively similar, but we must take into account that the physical processes involved are completely different.

In this work, we performed a quantitative experimental study on liquid−liquid PVME−PS polymer diffusion using confocal Raman microspectroscopy, a direct technique. The experimental method does not need any labeling and has been thoroughly analyzed and tested in earlier work.[27−29] By "optical sectioning", a direct observation of the interphase is possible with a moderate spatial resolution (in the order of microns). Differently from the ATR-FTIR technique extensively used for studying PS−PVME polymer interdiffusion, the whole composition profile can be directly observed, making its analysis and comparison with diffusion models easier. The system studied consists of a thin PVME-rich layer in contact with a thicker pure PS layer through a planar interface. Both PS and PVME samples used have very narrow molecular weight distributions. The diffusion process was monitored from very early stages (high diffusion rates) to very long times (when very low diffusion rates occur). Two diffusion temperatures were used as a crosscheck for the temperature dependencies of several thermodynamic and kinetics parameters used in the diffusion model calculations because they were taken from literature data. This experimental setup is expected to render precise and reliable information about the diffusion process.

The experimental data were compared with theoretical calculations from diffusion models based on physically realistic molecular models for the liquid dynamics and on sound thermodynamic principles. We considered two approaches that differ in the way that the monomeric friction coefficients are calculated. One of them is based on independent values for each polymer species, and these predictions agreed well with our experimental data. The other one is based on a common value for both monomeric friction coefficients, and the predictions of this approach did not agree with our experimental data.

Physical Diffusion Model Used

The details of a generalized model for liquid−liquid polymer diffusion in polydisperse systems can be found elsewhere.[30] In the present case, both components, PS and PVME, are nearly monodisperse. Therefore, the calculations of diffusion rates can be simplified considering a diffusion process with two components (PS and PVME) with polymerization degree l^{PVME} and l^{PS}, respectively. Under this assumption, the diffusion process can be modeled using a single binary diffusion coefficient (D)[4]

$$D = kT(\Phi^{PVME}\Lambda^{PS} + \Phi^{PS}\Lambda^{PVME})\left[\frac{\Phi^{PS}}{l^{PVME}} + \frac{\Phi^{PVME}}{l^{PS}} - 2\chi\Phi^{PS}\Phi^{PVME}\right] \quad (1)$$

where Φ represents concentrations (volume fractions), T temperature, Λ the Onsager coefficients, χ the thermodynamic interaction parameter, and k the Boltzmann constant. For the whole range of blend compositions selected for this work, the PVME sample has a molecular weight that is always below the critical molecular weight for entanglements. For this reason, Rouse-type dynamics is assumed for the PVME species and the Onsager coefficient for PVME becomes[2,4]

$$\Lambda_{PVME} = \frac{\Phi^{PVME}}{\zeta_0^{PVME}} \quad (2)$$

where ζ_0 represents the monomeric friction factor.

Key parameters used as input in the model calculations are the monomeric friction factors for PS and PVME and their dependences with composition and temperature. We considered two approaches proposed in the literature for obtaining these values. The "individual values approach" is based on independent values of the monomeric friction factors for PS and PVME. This approach is supported by experimental evidence on this particular system[17,19] as well as on other miscible blends[5] in the sense that the friction coefficients for each species may be very different. The use of independent values for the monomeric friction factors for every species present in the blend may imply the existence of more than a single glass-transition temperature (one for each species) and thermorheologically complex behavior, as each monomeric friction factor ought to follow a different WLF dependence. These issues have not been completely understood yet, and some experimental evidence indicates that the fact of whether this behavior can be observed or not depends on the particular species involved in the blend and on the experimental method used.[31−33]

For the "individual values approach", we used experimental data of the monomeric friction factor for PS and PVME calculated from tracer diffusion experiments by Green and others.[17,19] Values for the PS monomeric friction factor were taken from Figure 5 of ref 19. Values for the PVME monomeric friction factor were calculated using the procedure proposed and detailed in ref 17. The composition dependency of the monomeric friction factors (at constant $T - T_g$ blend = 107 K) were fitted in terms of the PVME volume fraction using the following expressions

$$\log \zeta_0^{PVME} = -7.041 + 8.858\Phi^{PVME} - 9.146(\Phi^{PVME})^2 \quad (3)$$

$$\log \zeta_0^{PS} = -6.437 + 10.961\Phi^{PVME} - 11.519(\Phi^{PVME})^2 \quad (4)$$

where the units for ζ_0 are [Dy·s/cm]. We assumed as a good approximation the use of a common T_g and WLF equation parameters for all species in the blend, as suggested by Figure 6 in ref 19 and by the work of Colby.[18] The WLF equation used to model the temperature dependence of friction factors was calculated converting the parameters of the Vogel−Fulcher form published in ref 19

$$\log\frac{\zeta_0(T_{ref})}{\zeta_0(T)} = \frac{-4.87(T - T_{ref})}{122.0 + T - T_{ref}} \quad (5)$$

where $T_{ref} = T_g + 107$ K. A low-degree polynomial was used to correlate precisely the composition dependence of the blend T_g, which was obtained by fitting experimental data obtained from DSC measurements on PS−PVME blends (see Experimental Section)

$$T_{g,blend} = 375.7 - 363.7\Phi^{PVME} + 313.0(\Phi^{PVME})^2 - 84.5(\Phi^{PVME})^3 \quad (6)$$

where the unit for $T_{g,blend}$ is K.

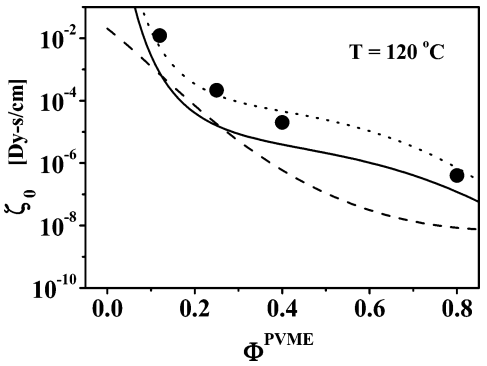

Figure 1. Monomeric friction coefficients used for diffusion simulations at 120 °C. (●) PS monomeric friction coefficient data, obtained from tracer diffusion experiments, taken from ref 19). (· · ·) PS monomeric friction coefficient data fit used for calculations. (—) PVME monomeric friction coefficient data fit used for calculations. (- - -) Common monomeric friction factor used for calculations taken from ref 22b.

A different approach, considering common values of friction coefficients for both PS and PVME components, was also examined. This "common value approach" may have been suggested by the viscosity−diffusion coefficient relationship existing in the Doi−Edwards model for homopolymer melts, as pointed out by Green and others. Doi−Edwards states that both the center of mass diffusion coefficient for the individual chain and the zero-shear viscosity for the melt depend on the same relaxation time and molecular structure parameters.[19,34] This concept was used by Jabbari and Peppas to calculate common monomeric friction values for both PS and PVME species. Starting from literature values for zero-shear viscosity for pure PS and pure PVME, a simple viscosity blending law was applied to calculate the PS−PVME blend viscosity values. From each blend composition, a common monomeric friction factor was calculated. These values, reported in ref 22b for two temperatures (105 and 125 °C), were used here for a second set of calculations

$$\log \bar{\zeta}_0(105\ °C) = 0.94 - 17.70\Phi^{PVME} + 7.99(\Phi^{PVME})^2 + 0.81(\Phi^{PVME})^3$$

$$\log \bar{\zeta}_0(125\ °C) = -2.50 - 10.54\Phi^{PVME} + 4.15(\Phi^{PVME})^2 + 0.55(\Phi^{PVME})^3 \quad (7)$$

To compare both approaches, we plotted in Figure 1 the calculated values for the monomeric friction factor (ζ_0) as a function of PVME volume fraction at 120 °C. The filled circles represent values experimentally measured by Green et al. for the PS monomeric friction factor, taken from Figure 2 of ref 19. The dotted and solid lines represent the values of ζ_0 for PS and PVME, calculated using eqs 3−6. The dashed line represents the common ζ_0 values calculated by Jabbari and Peppas,[22b] by the procedure described above as "common value approach".

Values of the Flory−Huggins thermodynamic interaction parameter (χ) for the PS−PVME polymer pair were taken from ref 15. The temperature dependence reported for this parameter (in the temperature range between 330 and 430 K) is given by

$$\chi = 0.0872 - \frac{35.86}{T} \quad (8)$$

where T is the absolute temperature [K].

To solve the continuity equations, we used the finite elements scheme detailed in ref 30. The restriction imposed by the mass conservation ($\Phi^{PS} + \Phi^{PVME} = 1$ at any point for any time) was explicitly included in the calculation scheme using a Lagrange multipliers strategy. Nonflux or Newmann boundary conditions were used at the outer surfaces of the sample.

Experimental Section

Materials Characterization. Polystyrene (sample P1505−St, M_n=217 000 g/mol, M_w/M_n=1.05) and poly(vinyl−methyl ether) (sample P2219-MVE, M_n =3850 g/mol, M_w/M_n =1.05) were purchased from Polymer Source (Dorval, Canada). Molecular weight characterization details were provided by the maker.

PS−PVME blends were prepared by weighing the polymers in the desired proportions, dissolving the solids in benzene at room temperature (about 10 % (w/w) solutions), and freeze-drying the necessary amounts of solutions. All samples were exhaustively dried under vacuum before using to remove any traces of solvent.

Glass-transition temperatures (T_g) for pure polymers and several PS−PVME blends (80%, 60%, 50%, 40%, and 20% PVME (w/w)) were measured by differential scanning calorimetry (DSC) using a Perkin-Elmer Pyris II DSC instrument. Samples were cooled and heated from −70 °C at rates of 10 °C/min under N_2 atmosphere. Glass-transition temperatures were determined as the onset of the transition. A single T_g was observed in all the PS−PVME blends. Experimental values of T_gs of PS−PVME blends were fitted as a function of the blend composition (PVME volume fraction) using a low-degree polynomial form (eq 6). This expression was used throughout this work for diffusion simulations.

Sample Preparation for Diffusion Experiments. Details of the samples used for the whole set of diffusion experiments, including layer compositions and thickness and diffusion temperatures, are given in Table 1. Two different compositions for the blends employed for the thin layers were used for the diffusion experiments conducted at 125 °C for the purpose of expanding the ($T - T_g$) range.

Composite plates for diffusion experiments were prepared as follows. A layer of pure PS (about 500 μm thick) was first prepared by vacuum molding, using cylindrical molds with sliding pistons. A thinner layer (between 40 and 80 μm thick) of a low-T_g PS−PVME blend was then vacuum molded on top of the thick PS layer. The molding temperature was conveniently chosen below the T_g of the thick layer to minimize diffusion at this stage. To avoid the sticky low-T_g blends to adhere to the metal piston, a highly polished, flat Teflon disk was placed on top of the low-T_g thin layer. After molding and cooling to room temperature, liquid nitrogen quenching produced an easy Teflon−low-T_g blend separation. Before performing the diffusion experiments, PVME composition profiles were measured to check for any amount of diffusion that might have occurred during the molding stage.

Diffusion between layers of the composite plates was promoted by elevating the temperature in a controlled oven (±0.5 °C) for specified times. The oven was continuously flushed with dry nitrogen to avoid sample oxidation. We kept the PS−PVME interface strictly horizontal all the time to prevent the flow of the high-viscosity thin layer. The samples were periodically removed from the oven for diffusion measurements and allowed to quickly cool to room temperature before Raman measurements were performed.

Confocal Raman Microspectroscopy. Local Raman spectra were measured at room temperature, on a Raman Microspectrometer DILOR LabRam Confocal, using a 16-mW He−Ne laser beam with a wavelength of 632.8 nm. The pinhole opening was between 100 and 300 μm (the maximum aperture is 1000 μm). In the excitation and collection path, an Olympus ×100 (NA=0.9) "dry" metallurgical objective was used. A slit opening of 500 μm and a holographic grating of 1800 lines/mm were used, which allows acquiring data in a Raman shift range between 500 and 1500 cm^{-1} with a spectral resolution of 4 cm^{-1}. The acquisition time for each spectrum was 100 s, and 10 spectra were accumulated for each data point.

Table 1. Characteristics of the Samples Used for Diffusion Experiments

	thin layer			thick layer		
sample	Φ^{PVME}	T_g [°C]	thickness [μ]	Φ^{PVME}	T_g [°C]	diffusion temp. [°C]
105-08	0.8	−30	72	0.0	100	105
125-08	0.8	−30	65	0.0	100	125
125-06	0.6	−21	95	0.0	100	125

The technique was used in the depth-profiling mode. Full details of this procedure have been detailed and discussed in earlier work.[28,29] The laser beam is aligned in a direction parallel to the diffusion coordinate and focused at successively deeper positions into the sample. The confocal device allows the "optical sectioning" of the sample, without physical cutting or microtoming. In this way, a large number of measurements—for many diffusion times—can be made without altering the sample; besides, this procedure eliminates uncertainties about experimental errors in the samples manufacture. As a disadvantage, if dry "metallurgical" microscope objectives are used, the actual spatial resolution of the method is worsened compared with that theoretically expected (1−2 μm). It is due to refraction of the laser beam at the air/polymer interface that enlarges the region of the sample illuminated by the laser beam, far beyond the diffraction limit.[28] The deeper one focuses into the sample, the larger the effect. In addition, the real focus point is placed deeper than the micrometric positioning screw; this effect increases linearly with depth. Both effects have been carefully analyzed in previous works and have been corrected in this work to obtain precise and reliable results.

After each diffusion period, local Raman spectra were measured along the diffusion coordinate. Spectra were acquired focusing the laser beam at different depths in steps of 2−5 μm (typically 30−40 measurements along the diffusion path). The composite plates were molded into specially designed sample holders, which allow a precise placement of the Raman laser beam, always at the same spot (within ±10 μm) of the sample surface.[29] Local chemical compositions were calculated from the acquired Raman spectra using the linear decomposition method.[35] A necessary calibration that relates Raman intensities with compositions was performed previously using the same blends prepared for DSC measurements.

Results and Discussion

Confocal Raman Measurements. Experimental results obtained from confocal Raman depth profiling at PVME-PS interphases, for samples annealed at 105 °C and 125 °C, are shown in Figure 2A,B. Results are presented in the form of PVME concentration profiles for several annealing times. Each profile was measured by focusing the laser beam at the outer surface of the PVME-rich layer and then recording local Raman spectra at successively deeper positions through this layer, up to the pure PS depth. The procedure was repeated for several annealing times, always focusing the laser beam at the same spot of the sample surface. In these plots, the zero at the abscissa scale (interdiffusion coordinate axis) corresponds to the outer surface of the PVME-rich layer.

The chemical composition profiles show clearly how the limited supply of PVME has diffused into the initially pure (thicker) PS layer. The limited PVME supply causes the PVME concentration at the thin (PVME-rich) layer to decrease with diffusion time. For both temperatures, it is observed that the PVME concentration at this region decreases rapidly at short times and then at lower rates at longer times. As will be shown later, the time evolution of this process reflects

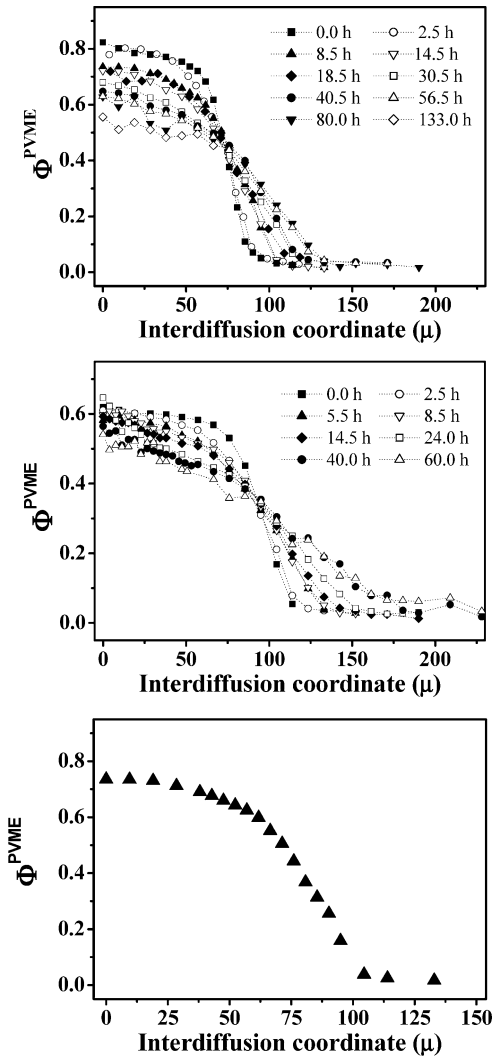

Figure 2. (A) Experimental PVME concentration profiles obtained from confocal Raman depth profiling at PS−PVME interphases for the sample 105-08 (annealed at 105 °C), measured for several annealing times, as indicated in the graph. (B) Experimental PVME concentration profiles obtained from confocal Raman depth profiling at PS−PVME interphases for the sample 125-06 (annealed at 125 °C), measured for several annealing times, as indicated in the graph. (C) Experimental results showing a representative PVME profile corresponding to the sample 105-08 after 8.5 h of diffusion at 105 °C.

the changes in local mobility as the local T_g approaches the temperature of the experiment and can be interpreted and precisely modeled in terms of the proposed diffusion model.

The profiles look different from the sigmoid complementary error functions, characteristic of Fickean diffusion with a constant diffusion coefficient. This feature can be better appreciated in Figure 2C, which shows a representative PVME concentration profile corresponding to the 105-08 sample after 8.5 h of diffusion at 105 °C. The general shape of these chemical composition profiles is markedly asymmetric and resembles the typical diffusion profiles between polymer pairs with different physical properties.[6,7,36] Moving from the outer surface of the PVME-rich layer along the diffusion path, the PVME concentration profile is at first fairly flat (the low-T_g region) and then its slope becomes increasingly higher, up to the pure PS layer (high-T_g region).

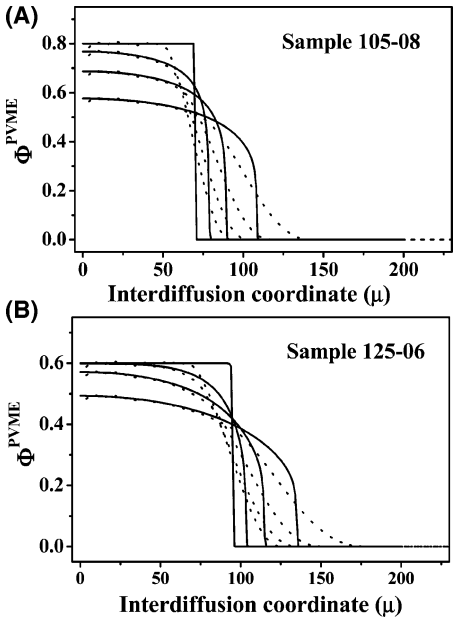

Figure 3. PVME concentration profiles calculated from the diffusion model. (—) Raw predictions based on the diffusion model, performed using the "individual values approach" for monomeric friction coefficient values. (· · ·) Model predictions convoluted with the instrumental spatial broadening function of the confocal Raman microspectrometer. (A) Sample 105-08 after 0, 2.5, 14.5, and 80 h of diffusion at 105 °C. (B) Sample 125-06 after 0, 2.5, 14.5, and 60 h of diffusion at 125 °C.

The characteristics described before can be clearly observed even while some fine details of the profiles, particularly the regions of higher slope close to the pure PS layer, are slightly distorted due to spatial resolution limitations of the experimental technique. At this point, the use of deconvolution would be a wise strategy to correct the artificial broadening because, for this case, the instrumental broadening function can be known in advance with a reasonable precision for a given set of instrumental conditions. This approach is currently under investigation. Instead, for the sake of better accuracy, we simulated the effect of the instrumental broadening by convoluting the diffusion model calculations, as will be developed in the next section.

Composition Profiles from Diffusion Models. The experimental results presented in the previous section can be compared with predictions from the diffusion model for the actual experimental conditions used (diffusion temperatures, initial thickness of the thin PVME-rich layer, and diffusion times).

PVME concentration profile results obtained from the diffusion model calculations corresponding to the samples 105-08 and 125-06 are shown in Figure 3A,B as solid lines for different diffusion times. Diffusion simulations were performed using the single binary diffusion coefficient given by eq 1, along with values of Flory thermodynamic interaction parameter calculated for each temperature using eq 8. The calculation results that we show were performed using the "individual values approach" based on independent values for the PS and PVME monomeric friction coefficients (eqs 3−6). Calculations performed using the "common values approach" (eq 7) rendered PVME composition profiles with similar characteristics (nonsymmetrical interphase composition profiles, due to abrupt changes of the monomeric friction factor along the PVME diffusion path) but predicted a much faster diffusion. This is due to the

much lower values for the monomeric friction coefficient predicted by the "common" approach, as shown in Figure 1. Also, the detailed changes of shape of the PVME concentration profile along the diffusion path ought to be somewhat different, but we can observe that the larger differences in Figure 1 are located in the PVME-rich region, which at the diffusion temperature has a relatively quite high diffusion coefficient. Therefore, the relative effect of using a common monomeric friction factor on the shape of the PVME concentration profile is diminished.

All the main characteristics already observed in the experimentally measured chemical composition profiles are also predicted by the diffusion model: The limited PVME supply causes the PVME concentration at the outer layer to decrease with diffusion time and a narrow interphase advances into the PS-rich layer, maintaining an almost rectangular-box shape for the PVME concentration profile. The highest slope region, associated with a higher T_g change, is located next to the glassy polymer (PS). The gradually decreasing slope reflects the influence of the T_g profile rapidly decreasing along the PS diffusion path, as explained in previous work.[7] The large variation of the monomeric friction coefficient with composition shown in Figure 1 leads to a very rapid decrease in the molecular mobility along the diffusion path and explains the asymmetry observed in calculated and experimentally measured PVME concentration profiles. This is a general pattern which we expect to be a common characteristic for every diffusion process involving liquid−liquid diffusion between polymers with very different molecular mobility, as is the present case.

To compare the diffusion model predictions with the experimental measurements, we simulated the instrumental resolution effects inherent to Raman depth-profiling by convoluting the theoretical predictions with the instrumental spatial broadening function.[28,29,37] As the convolution function we used the bell-shaped instrumental broadening function proposed in ref 33, which is characterized by a full-width at half-maximum (fwhm) that depends on the focusing depth. As a test for this procedure, we carried out in our laboratory additional experiments based on a different experimental design. We measured the Raman response (in depth-profiling mode) for a series of well-defined planar interfaces, which were carefully designed to serve as models for step changes in chemical composition profiles. The model step profiles, convoluted with the predicted instrumental broadening function, coincided with reasonable precision with the chemical composition profiles experimentally measured by depth profiling.[37] On the basis of those results, we are confident that the corrections introduced via convolution of the chemical composition profiles theoretically predicted are precise and realistic.

The PVME concentration profiles predicted by the diffusion model and convoluted with the instrumental broadening function are shown in Figure 3A,B as dotted lines. Even while they retain the main characteristics of the original profiles, the instrumental broadening affects mainly the regions with larger slopes, as the diffusion fronts (theoretically sharp), generating artificial tails. This effect is due to the fact that convoluting with a bell-shaped instrumental broadening function is somewhat similar to averaging the local chemical compositions over larger distances of the diffusion path.

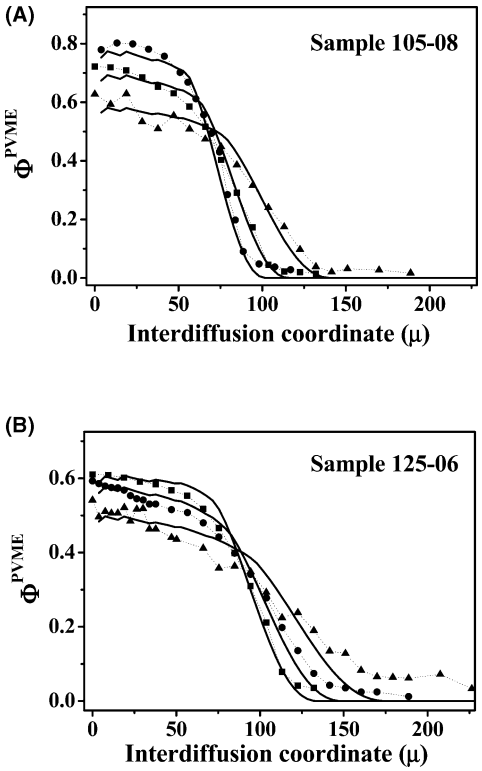

Figure 4. Comparison between experimental data (symbols) and model predictions (lines) for the same samples, diffusion temperatures, and diffusion times as those indicated in Figure 3. Calculations were performed using the "individual values approach" for the monomeric friction coefficient values.

Therefore, regions where the profiles have lower slopes are almost unaffected. In the next section, convoluted PVME concentration profiles will be compared with those experimentally measured.

Comparison between Experimental Profiles and Theoretical Predictions. Figure 4A,B is used to compare experimental measurements with the diffusion model predictions convoluted with the confocal Raman instrumental broadening curve for the same temperature and times as those shown in Figure 3A,B.

The convoluted simulation results are in excellent agreement with the experimental results within experimental error. The only differences observed between the predictions and the experimental data are the extension of some of the tails placed ahead of the diffusion fronts. Part of these differences is due to the finite size of the diffraction-limited volume of the sample from which Raman radiation is collected. Notice that when we corrected the decreasing in the depth resolution with the focusing depth, we assumed that refraction aberrations overwhelm diffraction effects and that the diffraction-limited volume that originates Raman radiation is infinitesimal.[28] However, the dimensions of this region are finite (depending on the microscope objective numerical aperture and on the wavelength of the laser beam). Even while the diffraction-limited volume is confined in a small region (2−5 μm), tails can be extended over tens of micrometers.[38] The rigorous correction of this effect involves a second convolution step and was not addressed in this work.[37] As explained before, the fact that the confocal Raman fwhm increases with the focusing depth causes—for larger focusing depths—somewhat larger differences between predicted values and experimental data. Experimental measurements for

depths beyond 125 μm in Figure 4B differ more with the convoluted model predictions, as expected.

The same combination of experimental methods and physical diffusion model was used to study liquid−liquid diffusion at the interphase between solid poly(phenylene oxide) (PPO) and liquid polystyrene (PS).[7] Those experiments performed with the PPO−PS pair are used as an extreme showcase to illustrate the importance of the markedly asymmetric interphase monomeric friction coefficient profiles to generate asymmetric interphase chemical composition profiles. The PS monomeric friction coefficient at the interphase rises by more than 10 orders of magnitude along the PS diffusion path, from the liquid PS to the solid PPO (see Figure 6 in ref 7). Striking similarities and large differences with the results shown at this work were found due to the solid PPO phase with high-yield stress that avoids liquid PS—with low osmotic pressure—to diffuse into the glassy matrix. The most important common characteristic is the nonsymmetric interphase chemical composition profiles found at the interphases where liquid−liquid polymer diffusion takes place. The same calculation procedure was used for the PPO−PS pair, and excellent agreement was also found between calculations and experimental results. For this work, the diffusion experimental conditions used amount to liquid−liquid diffusion between a low-viscosity liquid polymer (PVME) and a liquid polymer with very high viscosity (PS a few degrees above its T_g), and also markedly nonsymmetric interphase chemical composition profiles are found for a wide range of diffusion times. For all the experiments, the calculation results obtained by convoluting the diffusion model results with the instrumental spatial broadening curve agree very well with the direct, uncorrected experimental measurements.

Kinetics of the Diffusion Process. A method that has gained wide acceptance as a useful tool to follow the time evolution of the diffusion process in limited-supply experiments is the use of the chemical composition at the plateau region behind the advancing diffusion front.[29,39] Chemical composition at this plateau region is easier to measure and (for the case of confocal Raman spectroscopy) free from deviations caused by poor instrumental resolution conditions. Besides, the plateau region coincides with the chemical compositions associated to the largest mobility, and its time evolution is far more sensitive to the details of the diffusion model used. Earlier studies on the PS−PVME pair used a different approach to obtain data of the time evolution of the diffusion process. In these studies, an ill-conditioned summation of contributions from the deepest part of the advancing front was analyzed.[21,22] This type of ill-conditioned experimental information contains much larger experimental error and is therefore much harder to analyze. In addition, the slope of the advancing front is much less sensitive to the details of the diffusion model used because the main cause for the slowing down of the PVME advance is the large change of the local T_g and its effect on the monomeric friction coefficients.

Figure 5A,B shows the chemical composition at the plateau region behind the advancing diffusion front (in the form of PVME volume fractions) as a function of the diffusion time for the samples used in this work.

The experimental data shown correspond to averaged values for the outer 20 μm of the PVME-rich layer and are represented as symbols. Lines refer to calculations

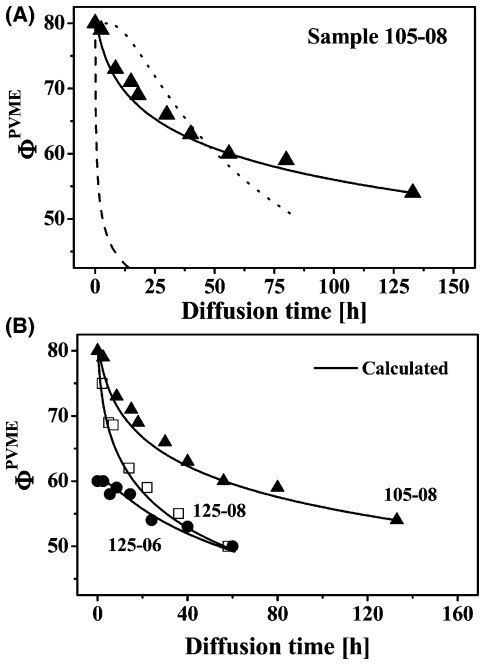

Figure 5. (A) Chemical composition of the plateau region behind the advancing diffusion front (in the form of PVME volume fractions) as a function of the diffusion time for sample 105-08. (▲) Experimental data: lines refer to model calculations; (a) (—) independent values for PS and PVME monomeric friction coefficients, (b) (· · ·) constant diffusion coefficient $D = 10^{-10}$ cm^2/s, (c) (- - -) common monomeric friction coefficient for PS and PVME. (B) Evolution of the PVME volume fraction at the plateau region behind the advancing diffusion front for all samples used. Symbols: experimentally measured values. Lines: diffusion model predictions using independent values for PS and PVME monomeric friction coefficients.

using diffusion models. Figure 5A shows experimental data corresponding to the 105-08 sample (diffusion at 105 °C) as solid triangles. Calculations carried out using a Fickean model with a constant diffusion coefficient ($D = 10^{-10}$ cm^2/s, dotted line) failed to reproduce the time evolution of the experimental data, as already established in earlier work.[21] Calculations using the diffusion model described above and independent monomeric friction coefficients for PVME and for PS (solid line) predict correctly the time evolution of the diffusion process. The use of a common monomeric friction coefficient (dashed line) overestimates the diffusion rates by a large error.

Figure 5B shows the comparisons of the diffusion model predictions (solid lines) with the full set of experimental data (symbols). Diffusion model calculations correspond to the "independent values approach". The agreement between experimental data and model predictions is excellent for the full range of diffusion times, thin layers starting chemical compositions and thickness, and diffusion temperatures studied. The diffusion experiments conducted with samples 125-08 and 125-06 were performed at the same diffusion temperature, and both samples show initial differences in T_g and thickness of the thin layers. Nevertheless, the experimentally measured PVME concentration at the plateau for these samples, after long diffusion times (in the order of 40 h), are virtually identical, as predicted by the model calculations. This fact also corresponds to the existence of a diffusion-controlling step at the liquid−liquid interphase that is in turn controlled by the diffusion temperature. Diffusion rates at the inter-

phase are the lowest for the whole PVME diffusion path, and therefore, the interphase controls the overall diffusion rate. The PVME is the faster diffusing species, and its mobility controls the whole diffusion process, as predicted elsewhere.[5]

To summarize, the results presented so far show that experimental data obtained for diffusion at the PVME-PS interphase are well predicted by the simple diffusion model proposed, only when experimental data on independent monomeric friction coefficients for both polymers are used for the calculations. The data show that the assumption of thermorheologically simple behavior (a common WLF equation for both components, PS and PVME) can be considered valid for diffusion experiments.

For miscible polymer blends, the local motion modes for each component species, which control the mobility of the individual chains, may not have either the same relaxation rate or the same temperature dependence. The energy barriers for main-chain bond rotations (intramolecular interactions), the size of the atoms set involved in that motion, and the intermolecular interactions between like and between different species together are expected to determine the chain T_g and the monomeric friction factor dependence on temperature.

The above-mentioned behavior cannot be generalized and may depend on the particular species pairs involved in the blends and on the experimental method used. The literature shows examples of remarkably simple behavior, as the polystyrene/polyisoprene blends. Polystyrene and polyisoprene have T_g differences well over 150 °C and show (to a good approximation) the same monomeric friction factors for PS and for PI, which depend only on the temperature interval above the matrix T_g.[40] In other cases, like the well-studied polystyrene (PS)−polyphenylene oxide (PPO) system,[5] the monomeric frictions coefficients for PS and PPO (obtained from tracer diffusion measurements) differ by more than 1 order of magnitude, even when compared at the same $T - T_g$ but share the same temperature dependence. After comparing Colby conclusions[18] and results from this work, we think that a similar behavior might be observed for other polymer pairs with thermorheological complex behavior for extended frequency ranges and a simple behavior for diffusion experiments. In an extreme case, Kim et al. measured tracer diffusion coefficients for the polystyrene−tetramethylbisphenol A polycarbonate (PS−TMPC) pair, where T_g values are separated about 100 °C, showing that the monomeric friction factor for TMPC can be more than 100 times larger than the monomeric friction coefficient for PS, and they follow different temperature dependences.[41] For the PS−PVME pair, the measurements made by Green have shown that PS and PVME monomeric friction factors are different and the temperature dependence for the blends viscosities and for the PS tracer diffusion coefficients are shown to be the same (see Figure 6 of ref 19).

Another issue that remains open is whether a common monomeric friction factor—calculated from blends zero-shear rate viscosities—can be used to describe polymer−polymer interdiffusion. At a first glance, one can expect that this type of calculation would render common monomeric friction coefficient values that could amount to some type of average for the individual monomeric friction coefficients for both species. Model calculations (not shown here) performed using a simple average for PS and PVME monomeric friction coefficients give a reasonable prediction for the whole diffusion experiments set. Similar calculations performed using the common monomeric friction coefficients reported in ref 22b clearly overestimate polymer diffusion, as shown in Figure 5A. We understand that the error is due to the rough approximations made by the authors to estimate blend viscosities because it has been experimentally shown that viscosity blending laws show large deviations from values experimentally measured for this polymers pair.[17] A much more complete study that ought to include the calculation of monomeric friction coefficient values from measurements of viscosities of PS−PVME blends may help to clarify this issue.

Conclusions

The experimental results obtained for diffusion at the interphase formed between liquid PVME and liquid PS were correctly predicted by a simple model for liquid−liquid polymer diffusion. The model assumes (a) simple and well-established liquid polymers molecular dynamics controlled by monomeric friction coefficients and (b) diffusive control by the faster diffusing species. The diffusion rate-controlling step is shown to be the PVME diffusion at the PS−PVME interphase. These results show that the need for combinations of Fickean and Case-II models, extensively used in previous works on this system, is clearly ruled out.

On the other hand, model predictions are in agreement with the experimental observations only when independent values for the monomeric friction factors for both PS and PVME (calculated from tracer diffusion experiments) were used in the diffusion calculations. The agreement is extended over a broad range of chemical compositions, local glass-transition temperatures, local molecular weight distributions, and monomeric friction coefficient values. Model predictions using a common value for the monomeric friction coefficients for both species, calculated from viscosity data taken from the literature, clearly did not follow the time evolution of the diffusion process. However, the issue of calculating common monomeric friction factors from blend viscosity data and its use for calculating liquid−liquid interdiffusion rates remains open, even while its physical meaning could not be clarified here.

Acknowledgment. Financial support from Agencia Nacional de Promoción de Ciencia y Tecnología (ANPCYT − PICT 14-07247) and Programa de Cooperación con Iberoamerica and CYTED (Project VIII-11) is acknowledged.

References and Notes

(1) Mills, P. J.; Green, P. F.; Palmstron, C. J.; Mayer, J. W.; Kramer, E. J. *J. Polym. Sci., Polym. Phys. Ed.* **1986**, *24*, 1.
(2) Tomba, J. P.; Carella, J. M. *J. Polym. Sci., Polym. Phys. Ed.* **1999**, *37*, 3097.
(3) Composto, R. J.; Kramer, E. J.; White, D. M. *Macromolecules* **1988**, *21*, 1, 2580.
(4) Kramer, E. J.; Green, P. F.; Palmstrom, C. J. *Polymer* **1984**, *25*, 473.
(5) Composto, R. J.; Kramer, E. J.; White, D. M. *Polymer* **1990**, *31*, 2320.
(6) Jordan, E. A.; Ball, R. C.; Donald, A. M.; Fetters, L. J.; Jones, R. A. L.; Klein, J. *Macromolecules* **1988**, *21* (1), 235.
(7) Tomba, J. P.; Carella, J. M.; García, D.; Pastor, J. M. *Macromolecules* **2001**, *34* (7), 2277.
(8) Tomba, J. P.; Carella, J. M.; Pardo E.; Lopez, S. *Macromol. Chem. Phys., Rapid Commun.* **2000**, *21* (14), 983−989.

(9) Bank, M.; Leffingwell, J.; Thies, C. *Macromolecules* **1971**, *4* (1), 43.
(10) Gelles, R.; Frank, C. W. *Macromolecules* **1983**, *16*, 1448.
(11) Yang, H.; Shibayama, M.; Stein, R.; Shimizu, N.; Hashimoto, T. *Macromolecules* **1986**, *19*, 1667.
(12) Kumaki, J.; Hashimoto, T. *Macromolecules* **1986**, *19*, 763.
(13) Ubrich, J. M.; Ben Cheikh Larbi, F.; Halary, J. L.; Monnerie, L.; Bauer, B. J.; Han, C. C. *Macromolecules* **1986**, *19*, 810.
(14) Han, C. C.; Bauer, B. J.; Clark, J. C.; Muroga, Y.; Matsushita, Y.; Okada, M.; Tran-cong, Q.; Chang, T. *Polymer* **1988**, *29*, 2002.
(15) Hammouda, B.; Briber, R. M.; Bauer, B. J. *Polymer* **1992**, *33* (8), 1785.
(16) Mazich, K. A. Ph.D. Thesis, Northwestern University, 1983.
(17) Green, P. F. *Macromolecules* **1991**, *24*, 3373.
(18) Pathak, J. A.; Colby, R. H.; Floudas, G.; Jerome, R. *Macromolecules* **1999**, *32*, 2553−2561.
(19) Green, P. F.; Adolf, D. B.; Gilliom, L. *Macromolecules* **1991**, *24*, 3377.
(20) Feng, Y.; Han, C. C.; Takenaka, M.; Hashimoto, T. *Polymer* **1992**, *33* (13), 2729.
(21) Jabbari, E.; Peppas, N. A. *Macromolecules* **1993**, *26* (9), 6229.
(22) (a) Jabbari, E.; Peppas, N. A. *J. Mater. Sci.* **1994**, *29*, 3969. (b) Jabbari, E.; Peppas, N. A. *Polymer* **1995**, *36* (3), 575. (c) Jabbari, E.; Peppas, N. A. *Macromolecules* **1995**, *28*, 6229.
(23) (a) Vaudreuil, S.; Qiu, H.; Kaliaguine, S.; Grmela, M.; Bousmina, M. *Macromol. Symp.* **2000**, *158*, 155. (b) Qiu, H.; Bousmina, M. *Macromolecules* **2000**, *33*, 6588.
(24) Thomas, N. L.; Windle, A. H. *Polymer* **1982**, *23*, 529.
(25) Hui, C.-Y.; Wu, K.-C.; Lasky, R. C.; Kramer, E. J. *J. Appl. Phys* **1987**, *61* (11), 5129.
(26) Hui, C.-Y.; Wu, K.-C.; Lasky, R. C.; Kramer, E. J. *J. Appl. Phys* **1987**, *61* (11), 5137.
(27) Meier, R. J.; Kip, B. J. *Microbeam Anal.* **1994**, *3*, 61.
(28) Everall, N. J. *Appl. Spectrosc.* **2000**, *54* (6), 773.
(29) Tomba, J. P.; Carella, J. M.; Pastor, J. M.;. Merino, J. C. *Polymer* **2002**, *43*, 6751.
(30) Pardo, E.; Tomba, J. P.; Carella, J. M. *Comput. Theor. Polym. Sci.* **2000**, *10* (6), 523.
(31) Kim, E.; Kramer, E. J.; Osby, J. O. *Macromolecules* **1995**, *28*, 1979.
(32) Colby, R. H. *Polymer* **1989**, *30*, 1275−1278.
(33) Milhaupt, J. M.; Lodge, T. P.; Smith, S. D.; Hamersky, M. W. *Macromolecules* **2001**, *34*, 5561.
(34) (a) Graessley, W. W. *J. Polym. Sci., Polym. Phys. Ed.* **1980**, *18*, 27. (b) Bartels, C. R.; Graessley, W. W.; Crist, B. J. *J. Polym. Sci., Polym. Lett.* **1983**, *21*, 495. (c) Bartels, C. R.; Graessley, W. W. *Macromolecules* **1984**, *17*, 7, 2702.
(35) Tomba, J. P.; De la Puente, E.; Pastor, J. M. *J. Polym. Sci., Part B: Polym. Phys.* **2000**, *38*, 1013.
(36) Composto, R. J.; Kramer E. J. *J. Mater. Sci.* **1991**, *26*, 2815.
(37) Tomba, J. P. *Appl. Spectrosc.*, submitted for publication.
(38) Meier, R. J, Kip, B. J. *Microbeam Anal.* **1994**, *3*, 61.
(39) (a) Nealy, P. F.; Cohen, R. E.; Argon, A. S. *Polymer* **1995**, *36* (19), 3687. (b) Zhou, Q.-Y.; Argon, A. S.; Cohen, R. E. *Polymer* **2001**, *42*, 613.
(40) (a) Chapman, B. R.; Hamersky, M. W.; Milhaupt, J. M.; Kostelecky, C.; Lodge, T. P.; von Meerwall, E. D.; Smith, S. D. *Macromolecules* **1998**, *31*, 4562. (b) Milhaupt, J. M.; Chapman, B. R.; Lodge, T. P.; Smith, S. D. *J. Polym. Sci., Polym. Phys. Ed.* **1998**, *36*, 3079.
(41) Kim, E.; Kramer, E. J.; Osby, J. O. *Macromolecules* **1995**, *28*, 1979.

MA0346052